https://doi.org/10.1016/j.biomaterials.2020.119931

Cartilage matrix-inspired biomimetic superlubricated nanospheres for treatment of osteoarthritis

Hao Chen; Tao Sun; Yufei Yan; Xiuling Ji; Yulong Sun; Xin Zhao; Jin Qi;Wenguo Cui*; Lianfu Deng*; Hongyu Zhang*

a State Key Laboratory of Tribology, Department of Mechanical Engineering, Tsinghua University, Beijing, 100084, China
b Shanghai Key Laboratory for Prevention and Treatment of Bone and Joint Diseases, Shanghai Institute of Traumatology and Orthopaedics, Ruijin Hospital, Shanghai Jiao Tong University School of Medicine, 197 Ruijin 2nd Road, Shanghai, 200025, PR China
c Department of Spinal Surgery, Renji Hospital, Shanghai Jiao Tong University School of Medicine, 160 Pujian Road, Shanghai, 200120, PR China
d Department of Biomedical Engineering, The Hong Kong Polytechnic University, Hung Hom, Hong Kong, China

Keywords: Biomimetic Articular cartilage Hydration lubrication Nanospheres Osteoarthritis

ABSTRACT
The superlubrication of natural joint has been attributed to hydration lubrication of articular cartilage. Here, inspired by the structure of phosphatidylcholine lipid (a typical cartilage matrix) with the presence of zwitterionic charges, we developed superlubricated nanospheres, namely poly (2-methacryloyloxyethyl phosphorylcholine)-grafted mesoporous silica nanospheres (MSNs-NH2@PMPC), via photopolymerization. The biomimetic nanospheres could enhance lubrication due to the formation of a tenacious hydration layer surrounding the zwitterionic charges of polymer brushes (PMPC), and achieve local delivery of an anti-inflammatory drug employing the nanocarriers (MSNs). The tribological and drug release tests showed improved lubrication and sustained drug release of the nanospheres. Additionally, the in vitro and in vivo tests revealed that the superlubricated drug-loaded nanospheres inhibited the development of osteoarthritis by up-regulating cartilage anabolic components and down-regulating catabolic proteases and pain-related gene. The nanospheres, with an integrated feature of both enhanced lubrication and sustained drug delivery, can be an efficient intra-articular nanomedicine for the treatment of osteoarthritis.

1. Introduction

In natural joint, articular cartilage consists of various biomacromolecules such as hyaluronic acid, aggrecan, lubricin, and phosphatidylcholine lipid. The zwitterionic headgroups of the phosphatidylcholine lipid can attract water molecules to form a tenacious hydration layer surrounding the charges [1], which will respond in a fluidlike manner when being sheared and thus result in a greatly reduced friction coefficient at the joint interface, typically at a level as low as 0.001–0.01 [2,3]. This mechanism, proposed by Klein et al. as hydration lubrication, has been accepted as the primary reason dominating the superlubrication property of the articular cartilage under pressure [4]. However, when the articular cartilage gradually degrades and causes higher friction, a self-reinforcing process will consequentially occur, which is considered as the origin for

the development of osteoarthritis [5]. The increased friction at the interface leads to high shear strain of the articular cartilage, which will be transmitted to the embedded superficial chondrocytes and then result in the up-regulation of cartilage-degrading enzymes, e.g. matrix metalloproteinases (MMP1), via a mechanotransduction mechanism [6,7]. Subsequently, the degraded articular cartilage (accelerated due to up-regulation of MMP1) is further abraded and removed upon sliding of the joint, resulting in even higher friction and increased expression of the cartilage□degrading enzymes. Consequently, the development of osteoarthritis is highly lubrication relevant, and the maintenance of joint superlubrication through a cartilage matrix-inspired design is crucial and the prerequisite to inhibit osteoarthritis [8].

Currently, two interventions are generally given to the patients for treatment of osteoarthritis, including intra-articular injection of hyaluronic acid and oral administration of glucosamine. These methods are performed with an aim to enhance joint lubrication or to promote cartilage repair [9]. However, it has been indicated that the viscosity of hyaluronic acid can dramatically decrease under high shear rate of joint motion, which is termed to be shear-thinning. Therefore, the function of hyaluronic acid as a lubrication-enhancing agent is much compromised because it cannot biomimic the hydration lubrication mechanism of phosphatidylcholine lipid [10]. In addition, it is anticipated that the anti-inflammatory drugs taken by oral administration are very difficult to reach the joint due to the lack of blood vessels in articular cartilage, which results in a considerably low absorption rate [11]. Therefore, these two interventions are, as a matter of fact, clinically ineffective. Consequently, developing a synergetic therapy for the treatment of osteoarthritis, which can achieve enhanced lubrication and sustained drug delivery, is greatly desirable [12,13]. From this point of view, it is meaningful to propose a design combining cartilage matrix-inspired superlubrication with efficient drug-loaded nanocarrier.

Poly (2-methacryloyloxyethyl phosphorylcholine) (PMPC) is a biocompatible polymer with the same zwitterionic charges ($N^+(CH3)_3$ and $PO4^-$) as phosphatidylcholine lipid, and it has been recognized as the most effective polyelectrolyte for hydration lubrication, attracting up to 15 or more water molecules within the hydration shell [14]. Previous studies on lubrication property of PMPC polymer brushes, either at a macro-scale [15–17] or at a micro-scale level [18,19], demonstrate that the friction coefficient between PMPC polymer brushes, which have been covalently bonded to the contact tribopairs, can be greatly reduced. Mesoporous silica nanospheres (MSNs) and other mesoporous materials have been widely used as a typical drug nanocarrier to achieve controlled and targeted drug delivery due to their highly odered pore structure, large surface area, large pore volume and the great feasibility for further surface modification [20–30]. Liu and Lu review the advances in multicompartment mesoporous silica micro/ nanostructures, ranging from core-shell and yolk-shell structures to Janus and raspberry-like nanoparticles, and discuss the important applications of the MSNs, including bioimaging, targeted drug/gene delivery, chemotherapy, phototherapy, and diagnostics [31]. Additionally, Another literature review performed by Stoddart and Zink indicates that the MSNs-based materials have great potential in many biomedical applications, especially in those situations where controlled and targeted drug delivery is preferably required [32]. Different approaches have been developed to graft functional polymers onto the surface of MSNs, among which photopolymerization is a versatile and low-toxic method without the involvement of complex synthesis procedure [33–35]. Consequently, grafting PMPC polymer brushes onto the surface of MSNs will produce an innovative type of nanospheres with lubrication enhancement and local drug delivery, which therefore can achieve a synergetic

treatment of osteoarthritis.

In the present study, bioinspired by hydration lubrication of phosphatidylcholine lipid, we successfully synthesize superlubricated nanospheres, namely PMPC polymer brushes-grafted MSNs (MSNs-NH2@ PMPC) via photopolymerization, and encapsulate an anti-inflammatory drug, diclofenac sodium (DS, widely used for osteoarthritis pain relief treatment), to prepare the lubrication-enhanced and drug-delivered MSNs (MSNs-NH2@PMPC-DS), as displayed in Fig. 1. We hypothesize that the dual-functional nanospheres developed herein can be used as a promising intra-articularly injected nanomedicine for synergetic treatment of osteoarthritis.

2. Materials and methods

2.1. Synthesis of MSNs-NH2@PMPC

The nanospheres MSNs and MSNs-NH2 (amino MSNs) were prepared with reference to our previous studies [36,37], and the photoinitiator was synthesized following a published protocol [38]. Briefly, 2-hydroxy-1-[4-(2-hydroxyethoxy)phenyl]-2-methyl-1-propanone (I2959, 0.12 mol), p-methyl benzene sulfonic chloride (TsCl, 0.10 mol) and KOH (0.40 mol) were dissolved in 300 mL of CH2Cl2 in a three necked round bottom flask. The solution was stirred at 25 °C for 2 h and washed three times with deionized water. The organic layer was dried over Na2SO4 and then distilled under vacuum. The resulting product was purified by silica gel (200–300 mesh) column chromatography, using ethyl acetate and methylene chloride (1:4, v/v) as an elution. The yield of the photoinitiator (I2959-Tos) was about 62.5%.

Subsequently, I2959-Tos (1 g), MSNs-NH2 (400 mg) and K2CO3 (2 g) were dissolved in 30 mL of N,N-dimethylformamide (DMF) in a round bottom flask, and the solution was stirred at 110 °C for 24 h. The resulting product was collected by centrifugation (8000 rpm, 15 min), washed sufficiently with DMF and deionized water, and then dried under vacuum overnight to obtain photoinitiator-immobilized nanospheres MSNs-NH2@I2959.

Finally, MSNs-NH2@I2959 (100 mg) and 2-methacryloyloxyethyl phosphorylcholine (MPC, 1 g) were uniformly dispersed in 10 mL of deionized water in a 50 mL round bottom flask. The solution was deoxygenated for 30 min, and photopolymerization was performed under UV-irradiation with an intensity of 5 mW/cm2 at 80 °C for 90 min. The resulting product was collected by centrifugation, washed sufficiently with ethanol/deionized water (1:1, v/v), and then dried under vacuum overnight to obtain the nanospheres MSNs-NH2@PMPC.

2.2. Characterizations of MSNs-NH2@PMPC

FTIR spectrum was recorded using a Nicolet 6700 spectrometer (Thermo Scientific, USA) at a wavelength from 400 cm^{-1} to 2500 cm^{-1} . XPS spectrum was recorded employing an escalab 250XI spectrometer (Thermo Scientific, USA) with the binding energy calibrated against O 1s peak at 523 eV. TGA was conducted on a Q5000IR instrument (TA Instruments, USA) at a heating rate of 10 °C/min from 25 °C to 800 °C. Surface morphology was examined using SEM (Quanta 200, FEI, Eindhoven, Netherlands) and TEM (JEM-2100F, FEI, JEOL, Japan). Hydrodynamic diameter was measured using a Zetasizer Nano ZS90 size analyzer (Malvern Instruments, UK) based on DLS technique. Specific surface area and pore volume data were obtained using an NOVA 4000 nitrogen adsorption and desorption instrument (Quantachrome Instruments, USA). Small angle XRD measurement was performed using a diffractometer (D8, Bruker, USA) at a scanning speed of

1°/min from 0.6° to 10°. The radiation source was copper (Kα1 = 1.54 Å).

2.3. Lubrication, rheology and adsorption properties

The lubrication property of MSNs-NH2@PMPC aqueous suspension was evaluated through a series of tribological tests. The tribological tests were performed using a UMT-3 universal materials tester (Centre for Tribology Inc., Campbell, California, USA) in a reciprocating mode (oscillation amplitude: 4 mm) at various concentrations (1–10 mg/mL) and frequencies (1–10 Hz), each for a duration of 30 min. A highly polished Ti6Al4V disk was used to be the lower specimen, which slid against a PE sphere pin (diameter: 8 mm), acting as the upper specimen. A normal load from 1 N to 4 N was applied, which was equivalent to an apparent maximum contact pressure of 26 MPa (1 N), 32 MPa (2 N), 37 MPa (3 N) and 41 MPa (4 N), respectively. This was calculated according to the Hertz equation for ball-on-flat configuration [39,40], where P is the apparent maximum contact pressure, F is the applied normal load, R is the radius of the PE sphere pin, E1 and μ1 are the elastic modulus and Poisson's ratio of Ti6Al4V (110 GPa, 0.3), and E2 and μ2 are the elastic modulus and Poisson's ratio of PE (1 GPa, 0.4).

$$P = \frac{1}{\pi}\sqrt[3]{\frac{6F}{\left(\frac{1-\mu_1^2}{E_1}+\frac{1-\mu_2^2}{E_2}\right)^2 R^2}} \qquad \text{(Eq. 1)}$$

The rheology property of MSNs-NH2@PMPC aqueous suspension was examined using a Physica MCR301 rheometer (Anton Paar, Austria) with a cone-and-plate module (diameter: 49.955 mm; cone angle: 0.988°). The amount of the MSNs-NH2@PMPC aqueous suspension dropped on the plate was 1.0 mL with different concentrations of 1 mg/mL, 2 mg/mL, 5 mg/mL and 10 mg/mL. The viscosity versus shear rate (1-1000 s^{-1}) curve was obtained under a shearing mode.

The adsorption property of MSNs-NH2@PMPC on Ti6Al4V disk was investigated as this was related with the lubrication mechanism of the nanospheres. Briefly, MSNs-NH2@PMPC (50 mg) were dispersed utrasonically in 10 mL of RhB aqueous solution (0.5 mM), and the mixture was stirred in a flask for 24 h. The RhB-labeled MSNs-NH2@ PMPC were collected through centrifugation, washed sufficiently with deionized water, and then dried under vacuum at room temperature. Subsequently, the RhB-labeled MSNs-NH2@PMPC were redispersed, and a drop of suspension was placed on the Ti6Al4V disk. After incubation for 1 h, the Ti6Al4V disk was washed with deionized water and dried by nitrogen flow. Finally, the adsorption of RhB-labeled MSNs-NH2@PMPC on the Ti6Al4V disk was observed using a Leica DM6000B fluorescence microscopy (Wetzlar, Germany). The adsorption property of RhB-labeled MSNs-NH2@PMPC at a concentration of 10 mg/mL was also investigated using the same method.

2.4. In vitro drug loading and release behavior

DS was dissolved in PBS (pH = 7.4) at different concentrations, and the calibration curve was obtained by recording the absorbance of the solutions with a UV–vis spectrophotometer (UV-6100s, Metash Instruments, China) at 276 nm, as shown in Fig. 4a. MSNs-NH2@PMPC (20 mg) were added to 10 mL of DS solution (0.5 mM) in PBS, dispersed uniformly by ultrasound, and stirred for 48 h at room temperature. The DS-loaded nanospheres were collected through centrifugation (8000 rpm, 5 min), washed sufficiently with deionized water, and then dried under vacuum overnight. The DS-loaded MSNs were prepared using the same method. The amount of DS in the solution was analyzed using the UV–vis spectrophotometer to calculate drug loading capacity (LC) and encapsulation efficiency (EE), which were obtained according to the following equations.

$$LC(\%)_{MSNs} = \frac{amount\ of\ loaded\ DS}{amount\ of\ DS - loaded\ MSNs} \times 100 \quad \text{(Eq. 2)}$$

$$LC(\%)_{MSNs-NH_2@PMPC} = \frac{amount\ of\ loaded\ DS}{amount\ of\ DS - loaded\ MSNs - NH_2@PMPC} \times 100 \quad \text{(Eq. 3)}$$

$$EE(\%) = \frac{amount\ of\ loaded\ DS}{amount\ of\ added\ DS} \times 100 \quad \text{(Eq. 4)}$$

The release of DS from MSNs and MSNs-NH2@PMPC was investigated through dialysis tube diffusion over a duration of 72 h. Briefly, 20 mg of DS-loaded MSNs and 20 mg of DS-loaded MSNs-NH2@ PMPC were dispersed uniformly in 10 mL of PBS, and 2 mL of each suspension was put into a dialysis tube (molecular weight cutoff: 8000–10000). Subsequently, the tube was dialyzed in 20 mL of PBS at 37 °C. Following a predetermined time, 2 mL of the medium was removed from the release buffer and replaced by 2 mL of fresh PBS. Finally, the amount of DS released from the nanospheres was evaluated by the UV–vis spectrophotometer, and the drug release profile was drawn accordingly.

2.5. In vitro cell cytotoxicity

Chondrocytes were isolated from the knees of Sprague Dawley rats. The cartilage tissue was minced by scissors, cut into small fragments (< 1 mm3), and washed thoroughly with PBS for three times. The tissue fragments were digested by 0.25% trypsin for 30 min and then by 0.2% type II collagenase at 37 °C for another 4 h. The released chondrocytes were washed with PBS, and cultured in the Dulbecco's Modified Eagle Medium/Nutrient Mixture F-12 (DMEM/F12) supplemented with 10% fetal bovine serum and 1% antibiotics in an incubator (37 °C and 5% CO2). When reaching at 70–80% confluency, chondrocytes were harvested by trypsinization with 0.05% trypsin-EDTA and split as 1:3 to a new culture dish. The cells at passages 3–6 were used in the following experiments, and the sterilized nanospheres were added into the culture medium with the final concentration of 5% (w/v). The sterilized nanospheres were obtained by soaking into 75% ethanol for 5 min and washing thoroughly with sterilized PBS. As only a tiny amount of DS can be released during the sterilization process, it is considered that the biological effect of the drug is not affected.

CCK-8 (Donjindo, Japan) assay was employed to evaluate cell proliferation and cytotoxicity. Chondrocytes were seeded into a 96-well plate at a density of 104 cells/mL with or without the nanospheres. The plate was incubated in the incubator at 37 °C and 5% CO2. After culturing for 1, 3 and 5 days, 10 μL of CCK-8 solution was added into each well of the plate, and then the cells were cultured for another 2 h. The absorbance of the solution was measured using a microplate reader (Infinite F50, Tecan, Switzerland) at a wavelength of 450 nm. In addition, the cell viability of chondrocytes was examined using Live/Dead staining assay (Thermo Fisher, USA), which stains the live cells with green fluorescence (calcein-AM) and the dead cells with red fluorescence (ethidium homodimer-1). Briefly, after the chondrocytes were cultured for 1, 3 and 5 days with or without the nanospheres, the culture medium was removed and the cells were washed thoroughly with PBS. The dye solution was added into each well of the plate, and the cells were incubated for another 20 min prior to observation using a laser scanning confocal microscope (LSCM, LSM-800, ZEISS, Germany).

2.6. qRT-PCR analysis

Chondrocytes were seeded into 6-well plates at a density of 5 × 105 cells/mL, treated with 10 mU of H2O2, and co-cultured with MSNs, MSNs-DS, MSNs-NH2@PMPC, MSNs-NH2@PMPC-DS and DS for 24 h. The total RNA from the cells was extracted using TRIzol reagent (Invitrogen, USA) according to the manufacturer's protocol. RNA con□centration and purity were determined via measuring the absorbance at 260 nm and 280 nm, respectively. Complementary DNA (cDNA) was synthesized using 1 μg of RNA and a Reverse Transcription System Kit (TaKaRa, China). qRT-PCR was performed to amplify cDNA using a SYBR Premix Ex Tag Kit (TaKaRa, China) and an ABI 7500 Sequencing Detection System (Applied Biosystems, USA). The expression levels of mRNA including Col2α, aggrecan (AGG), MMP1, TAC1 and GAPDH were determined using specific primers and normalized to GAPDH. The primer sequences used in this study were as follows. GAPDH: forward, 5′-GAAGGTCGGTGTGAACGGATTTG-3'; reverse, 5′-CATGTAGACCATG TAGTTGAGGTCA-3'; Col2α: forward, 5′-CTCAAGTCGCTGAACAACCA 3'; reverse, 5′-GTCTCCGCTCTTCCACTCTG-3'; aggrecan: forward, 5′-GATCTCAGTGGGCAACCTTC-3'; reverse, 5′- TCCACAAACGTAATGC CAGA-3'; MMP1: forward, 5′-CACTCCCTTGGACTCACTCA -3'; reverse, 5′-CCCATATAAAGCCTGGATGC-3'; TAC1: forward, 5′- TTGCAGAGGA AATCGGTGCC-3'; reverse, 5′-GAACTGCTGAGGCTTGGGTC-3'.

2.7. Immunofluorescence staining

Chondrocytes were seeded onto sterile glass coverslips in 24-well plates at a density of 5 × 104 cells per well, treated with 10 mU of H2O2, and co-cultured with MSNs, MSNs-NH2@PMPC and MSNs-NH2@ PMPC-DS for 12 h. After incubation, the cells were washed with PBS, fixed in 4% paraformaldehyde for 10 min, treated with 0.1% Triton X100 for 15 min, and incubated in 3% bovine serum albumin/PBS for 30 min at room temperature. Subsequently, the cells were washed with PBS and incubated with rat primary anti-Col2α antibody (Abcam, 1:200 dilution) at 4 °C overnight. After incubation, the cells were washed with PBS again and incubated with appropriate Alexa Fluor conjugated secondary antibodies (Molecular Probes, Life Tech, USA, 1:400 dilution) at room temperature for 1 h. The 4, 6-diamidino-2-phenyindole dilactate (DAPI, Life Tech, USA) and Alexa Fluor 594 phalloidin (Life Tech, USA) were used to counterstain cellular nuclei and actin rings, respectively. The immunofluorescence images were acquired by using the laser scanning confocal microscopy. The protein expression level of Col2α was also acquired based on the fluorescence intensity of the images for quantitative comparison using Image J software.

2.8. Rat osteoarthritis model and surgical treatment

The animal study was approved by the Animal Research Committee of Ruijin Hospital, School of Medicine, Shanghai Jiaotong University, China, and it was in compliance with the National Institutes of Health Guidelines for the Care and Use of Laboratory Animals. Sprague Dawley rats (12 weeks old, n = 24) were used to create an osteoarthritis model via the DMM surgery (Fig. S1a). Briefly, the rats were anesthetized with pentobarbital sodium by intraperitoneal injection (30 mg/kg body weight), and then a skin incision was made from the distal patella to the proximal tibial plateau in the right knee joint. The joint capsule immediately medial to the patellar tendon was incised and spread open with scissors. Afterward, the patellar tendon was retracted, and the cranial meniscotibial ligament of the medial meniscus (MMTL) was exposed through blunt dissection of the fat pad. The MMTL was sectioned using a micro-surgical knife, and then the wound was closed cutaneously. The rats were provided with free access to food and water, and allowed for unrestricted activity

every day. The rats were randomly sorted into four groups (n = 3 for each group), and intra-articularly injected with MSNs, MSNs-DS, MSNs-NH2@PMPC and MSNs-NH2@ PMPC-DS (concentration of all the materials: 10 mg/mL) once a week. The rats received a running train on a level treadmill at a speed of 20 m/min for 1 h every other day to induce osteoarthritis of the knee joint (Fig. S1b).

2.9. X-ray radiography and micro-CT arthrography

The rats received an X-ray scanning by employing an X-ray imager for small animals (Faxitron X-ray, USA) at 2 and 4 weeks after the DMM surgery. The scanning was performed with a voltage of 32 kV and an exposure time of 6 mA s. The articular space width of rat knee joints was measured based on the X-ray radiographs. In addition, the rats were sacrificed at 2 and 4 weeks after the DMM surgery, and the knee joint samples were obtained for an arthrography using a high resolution micro-CT imaging system (SkyScan 1172, Bruker BioSpin, Belgium). The relative osteophytes volume was evaluated based on the result of micro-CT scanning and reconstruction.

2.10. Histological staining and immunohistochemistry staining

The knee joints were fixed in 4% paraformaldehyde, decalcified in 10% EDTA, dehydrated in ethanol and embedded in paraffin. Serial paraffin sections (thickness: 5 μm) were prepared for histological staining. H&E staining and Safranin O-fast green staining were used to evaluate histopathological features and make scores according to the OARSI criterion established by Pritzker et al. [41]. The digital images were captured, and two of the authors (Chen and Qi) graded the sections independently. Additionally, the relative glycosaminoglycan content was measured based on the safranin O-fast green staining using Image J software.

Regarding immunohistochemistry staining, the paraffin sections of the cartilage tissue were deparaffinized in xylene, hydrated in ethanol, and rinsed in distilled water. Afterward, the sections were rinsed using PBST (PBS with Tween-20) and incubated with normal serum block. The sections were incubated with rat primary and secondary anti-Col2α antibodies using the same procedure as mentioned above. DAPI was used to counterstain cellular nuclei, and the sections were covered by using a coverslip with anti-fade mounting medium. The fluorescence images were obtained by the laser scanning confocal microscopy, and the protein expression level of Col2α was acquired based on the fluorescence intensity of the images using Image J software.

2.11. Statistical analysis

The experiments were repeated three times to verify the results, and the assays were performed at least in triplicate. The data were expressed as mean ± SD, and one-way analysis of variance (ANOVA) with Turkey post-test was used for the multiple comparison tests. A two-tailed non-paired Student's t-test was used to compare the difference between two groups, and statistical significance was displayed as *$P < 0.05$, **$P < 0.01$ and ***$P < 0.001$; #$P < 0.05$, ##$P < 0.01$ and ###$P < 0.001$. The statistical analysis was conducted by using the GraphPad Prism software (Version 5.0, GraphPad Software Inc., USA).

3. Results and discussion

3.1. Preparation of lubrication-enhanced and drug-delivered nanospheres

We successfully developed innovative lubrication-enhanced and drug-delivered nanospheres

(MSNs-NH2@PMPC-DS), as an intra-articularly injected nanomedicine, for the treatment of osteoarthritis. The design of the nanospheres was inspired by the superlubrication property of articular cartilage matrix, specifically the zwitterionic charges of phosphatidylcholine lipid. The enhanced lubrication of MSNs-NH2@ PMPC-DS was achieved by using PMPC polymer brushes based on hydration lubrication, while simultaneously the sustained drug delivery was accomplished by using MSNs as an effective drug nanocarrier. The biomimetic super lubricated nanospheres were synthesized through photopolymerization, as shown in Fig. 1a. Firstly, the photoinitiator (I2959-Tos) was synthesized and modified onto the surface of MSNsNH2 by substitution reaction, with the resulting product named as MSNs-NH2@I2959. Afterward, MSNs-NH2@I2959 were uniformly dispersed in the monomer solution under UV-irradiation, and MSNs-NH2@ PMPC nanospheres were synthesized through photopolymerization without introduction of any toxic materials. The density and length of PMPC polymer brushes grafted on the surface of MSNs were calculated to be 1.4/nm2 and 4.3 nm (Supporting Information). Finally, an anti-inflammatory drug (DS) was encapsulated into the MSNs-NH2@PMPC in order to prepare the lubrication-enhanced and drug-delivered dual□functional nanospheres (MSNs-NH2@PMPC-DS). Conventional methods to synthesize polymer-grafted MSNs, for example the surface-initiated atom transfer radical polymerization, is commonly criticized for high polymerization temperature, complicated synthesis procedure and the residue of transition metal ions [42,43]. Specifically, the residue of transition metal ions is undesirable and may compromise the application in biomedical field. The photopolymerization approach developed in this study, with the use of biocompatible PMPC polymer brushes and MSNs nanocarriers, is a versatile and low-toxic method, which represents a promising strategy to prepare functional nanomaterials for various biomedical applications. Additionally, it is considered that the dual-functional nanospheres (MSNs-NH2@PMPC-DS) have good stability as the main components, MSNs and PMPC, are not biodegradable and can be used in various biomedical applications [15–17,30,31]. Therefore, the material stability is not examined in the present study.

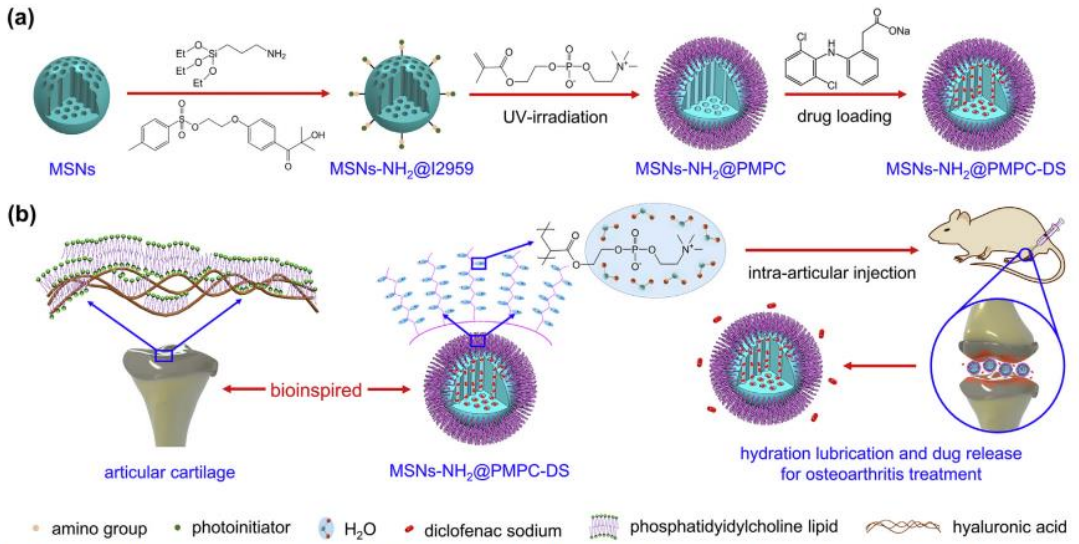

Fig. 1. Schematic illustration of biomimetic superlubricated nanospheres. (a) Synthesis of the biomimetic superlubricated drug-loaded nanospheres via photo-polymerization. (b) Design of the superlubricated nanospheres, which is bioinspired by hydration lubrication mechanism of phosphatidylcholine lipid, and the synergetic treatment of osteoarthritis based on enhanced lubrication and sustained drug release.

3.2. Nanospheres characterizations

In order to confirm that the cartilage matrix-inspired PMPC polymer brushes (with the same

zwitterionic charges as phosphatidylcholine lipid) had been successfully grafted onto the surface of MSNs, Fourier transform infrared (FTIR) spectrum, X-ray photoelectron spectrum (XPS) and thermogravimetric analysis (TGA) of MSNs, MSNs-NH2, MSNs-NH2@I2959 and MSNs-NH2@PMPC were performed. The FTIR spectra of the nanospheres are presented in Fig. 2a. The Si–O–Si absorption peak of the nanospheres appears at 1093 cm^{-1} . The peak at 1560 cm^{-1} of MSNs-NH2 is attributed to $–NH_2$ asymmetric bending vibration, and the peak at 1500–1600 cm^{-1} of MSNs-NH2@I2959 is attributed to benzene skeleton vibration. The peaks of P–O, P]O and C]O for MSNs-NH2@PMPC appear at 964 cm−1 , 1244 cm−1 and 1725 cm−1 , respectively. The XPS of the nanospheres is shown in Fig. 2b. The binding energies of Si 2p and Si 2s for MSNs are at 104 eV and 155 eV. The binding energy of N 1s for MSNs-NH2 and MSNs-NH2@ I2959 due to the presence of amine groups is at 398 eV, and the binding energies of P 2p and P 2s for MSNs-NH2@PMPC are at 131 eV and 189 eV. The TGA results of the nanospheres are demonstrated in Fig. 2c. The weight loss of MSNs is 6.4%, and it dramatically increases to 12.9%, 14.2% and 33.1% for MSNs-NH2, MSNs-NH2@I2959 and MSNsNH2@PMPC, respectively. Quantitatively, it can be calculated that the contents of the photoinitiator in MSNs-NH2@I2959 and the PMPC polymer brushes in MSNs-NH2@PMPC are about 1.5% and 22.0%.

Scanning electron microscopy (SEM), transmission electron microscopy (TEM) and dynamic light scattering (DLS) of MSNs and MSNsNH2@PMPC were performed to characterize the surface morphology and hydrodynamic diameter of the developed nanospheres. The surface morphology of MSNs and MSNs-NH2@PMPC is shown in Fig. 2d and e. MSNs are spherical in shape and exhibit homogeneous ordered meso□porous structure. Following surface grafting of PMPC polymer brushes, MSNs-NH2@PMPC demonstrate a typical shaded layer surrounding the nanospheres, with a thickness of approximately 6 nm. The hydrodynamic diameter of MSNs and MSNs-NH2@PMPC is presented in Fig. 2f, which increases dramatically from 180 nm to 260 nm. It is noted that the hydrodynamic diameter measured by DLS is larger than that of morphological observation due to the hydration effect of the PMPC polymer brushes, which are well stretched in aqueous solution.

Nitrogen adsorption-desorption isotherm and X-ray diffraction (XRD) pattern of MSNs and MSNs-NH2@PMPC were performed to evaluate the mesoporous properties of the developed nanospheres. The typical nitrogen adsorption-desorption isotherm and pore size distribution of MSNs and MSNs-NH2@PMPC are illustrated in Fig. 2g and h. The isotherms correspond to the type IV pattern, with the presence of a hysteresis loop. The specific surface area and pore volume are calculated based on Brunauer-Emmett-Teller (BET) and Barrett-Joyner Halenda (BJH) method, which decrease greatly from 805 m2 /g and 0.81 mL/g (MSNs) to 50 m2 /g and 0.10 mL/g (MSNs-NH2@PMPC), as shown in Table S1. In comparison with MSNs, the great reduction in specific surface area and pore volume of MSNs-NH2@PMPC indicates that the mesoporous channels of the nanospheres are almost blocked by the PMPC polymer brushes. The XRD patterns of MSNs, MSNs-NH2, MSNs-NH2@I2959 and MSNs-NH2@PMPC are displayed in Fig. 2i. MSNs demonstrate standard Bragg peaks of (100), (110) and (200), indicating a highly ordered hexagonal array. Following surface grafting of the PMPC polymer brushes, the Bragg peak of (100) is still slightly visible while the Bragg peaks of (110) and (200) disappear for MSNsNH2@PMPC, which is attributed to the relative weak crystallinity of the PMPC polymer brushes. Furthermore, the distances between adjacent pores of MSNs and MSNs-NH2@PMPC are calculated based on the Bragg equation: $2d \sin\theta = n\lambda$. The (100) peak interplanar spacing $d100 = n\lambda/(2 \sin\theta)$. Therefore, the pore distance $a = (2/1.732)\, d100 = 1.155\lambda/(2 \sin\theta)$, where $n = 1$; $\lambda = 1.54$ Å. Consequently, the

interplanar spacing and pore distance of MSNs and MSNs-NH2@PMPC are summarized in Table S1.

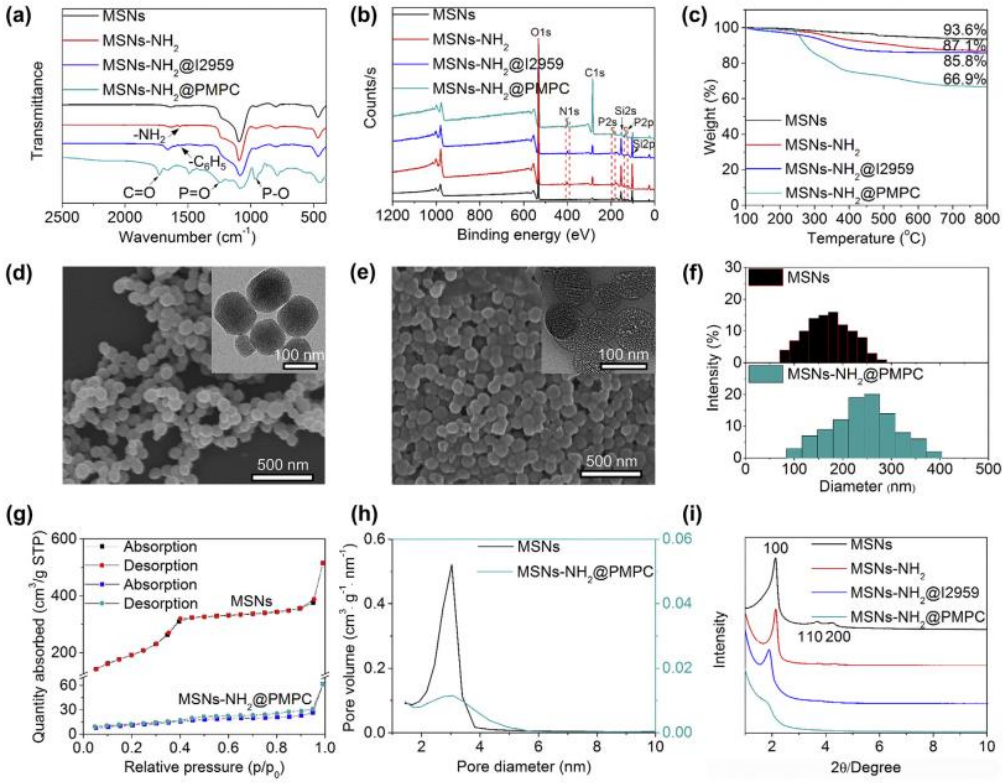

Fig. 2. Characterizations of the nanospheres. (a) FTIR spectra, (b) XPS spectra, and (c) TGA curves of MSNs, MSNs-NH_2, MSNs-NH_2@I2959 and MSNs-NH_2@PMPC. (d–e) SEM and TEM images (insert) of MSNs and MSNs-NH_2@PMPC. (f) Hydrodynamic diameters of MSNs and MSNs-NH_2@PMPC measured by DLS. (g) Nitrogen adsorption-desorption isotherms, and (h) pore size distribution curves of MSNs and MSNs-NH_2@PMPC. (i) XRD patterns of MSNs, MSNs-NH_2, MSNs-NH_2@I2959 and MSNs-NH_2@PMPC.

3.3. Lubrication, rheology, adsorption and drug loading and release properties

The lubrication property of the MSNs-NH2@PMPC aqueous suspension tested under various conditions is shown in Fig. 3. Fig. 3a displays the friction coefficient-time plots for the contact pairs lubricated by deionized water, MSNs (10 mg/mL) and MSNs-NH2@PMPC (10 mg/mL). The applied normal load is 3 N, and the reciprocating frequency is 3 Hz. Compared with deionized water (0.06) and MSNs (0.07), the friction coefficient for MSNs-NH2@PMPC decreases significantly (0.017). It is noted that no lubrication effect is observed when MSNs is used to be the lubricant. Fig. 3b illustrates the friction coefficient-time plots lubricated by MSNs-NH2@PMPC at different concentrations (1–10 mg/mL) under an applied normal load of 3 N and a reciprocating frequency of 3 Hz. The friction coefficient of MSNsNH2@PMPC decreases gradually with the increase in concentration (1 mg/mL: 0.052; 2 mg/mL: 0.036; 5 mg/mL: 0.018; 10 mg/mL: 0.017) and is much smaller than that of deionized water. Fig. 3c presents the friction coefficient-time plots lubricated by MSNs-NH2@PMPC (10 mg/ mL) at different reciprocating frequencies (1–10 Hz) under an applied normal load of 3 N. There seems to be a decreasing trend with the increase in reciprocating frequency (1 Hz: 0.029; 3 Hz: 0.017; 5 Hz: 0.017; 10 Hz: 0.013). Fig. 3d demonstrates the friction coefficient-time plots lubricated by MSNs-NH2@PMPC (10 mg/mL) at different applied normal loads (1–4 N, equivalent to the apparent maximum contact pressures of 26–41 MPa [44,45], which are much higher than the typical pressure at the human joint [4], ~5 MPa) under a reciprocating frequency of 3 Hz. The friction coefficient remains at a low level for all the applied normal loads (1 N: 0.02; 2 N: 0.024; 3 N: 0.017; 4 N: 0.015). Fig. 3e shows the friction coefficient-time plot

lubricated by MSNs□NH2@PMPC with an extended duration of 90 min (applied normal load: 3 N; reciprocating frequency: 3 Hz; concentration: 10 mg/mL), and the friction coefficient remains stable during the test.

It is considered based on the lubrication property of the MSNsNH2@PMPC aqueous suspension that the novel nanospheres may be employed as an effective lubricant to enhance lubrication of the joint and thus relieve the pain caused by osteoarthritis. Theoretically, the zwitterionic PMPC polymer brushes in MSNs-NH2@PMPC are sufficiently stretched in aqueous conditions and form a tenaciously attached hydration layer surrounding the positive ($N+(CH_3)_3$) and negative ($PO4^-$) charges due to a large interaction between the water dipole and the enclosed zwitterionic charges. The hydration layer can not only support high pressures without being squeezed out but also transform into a relaxation phase very rapidly, resulting in a fluidlike response to shear and significantly reducing interfacial friction via hydration lubrication [14]. The same mechanism has been accepted as the scenario for superlubrication of articular cartilage, which is achieved by the zwitterionic charges in phosphatidylcholine lipid. In order to confirm the detailed lubrication mechanism, the wear scar area after the tribological test using MSNs and MSNs-NH2@PMPC aqueous suspensions (applied normal load: 3 N; concentration: 10 mg/mL; reciprocating frequency: 3 Hz) is investigated by SEM (Fig. 3g and h), which is associated with an energy dispersive X-ray (EDX) analysis (Fig. 3i). When MSNs is used to be the lubricant, it conforms to abrasive wear due to the presence of typical grooves within the wear scar area. Furthermore, EDX analysis shows a small amount of Si element in the wear scar, indicating that the MSNs function as abrasive nanospheres during the tribological test. On the contrary, the wear scar area appears relatively smooth, and few wear grooves are observed when MSNs-NH2@PMPC is used as the lubricant, which demonstrates that the PMPC polymer brushes efficiently decrease abrasive wear and enhance lubrication between the contact tribopairs.

The rheological property of MSNs-NH2@PMPC aqueous suspension (1 mg/mL, 2 mg/mL, 5 mg/mL and 10 mg/mL) depicted by viscosity versus shear rate curve is presented in Fig. 3f. The viscosity shows a slightly increasing trend with the increase in shear rate, conforming to the typical feature of shear-thickening behavior of non-Newtonian fluid. This result is in good agreement with the findings of a previous study, in which a shear-thickening phenomenon is also observed for an aqueous suspension with the ploy (3-sulfopropyl methacrylate potassium salt)-grafted hollow silica nanoparticles as the lubricant additive [12]. Currently, hyaluronic acid is clinically used as an intraarticularly injected viscosupplement to alleviate pain for the patients suffering from osteoarthritis. However, hyaluronic acid is shear-thinning at the concentration similar to synovial fluid, as a result the viscosity becomes comparable to that of water under typical shear rates across the sliding articular cartilage surface (which can reach 10^{5-6} s^{-1}) and thus has limited lubrication effect [10,14]. From this point of view, the MSNs-NH2@PMPC developed in this study, with a shear□thickening property under high shear rate, is beneficial as an intra-articularly injected lubricant for the treatment of osteoarthritis.

The fluorescence images of the Ti6Al4V surface incubated with Rhodamine B (RhB)-labeled MSNs-NH2@PMPC are shown in Fig. 3j-l, with the bare Ti6Al4V surface as control. Only a tiny amount of sparsely distributed fluorescence spots are detected at the concentration of 5 mg/mL, and the number of fluorescence spots increases greatly at a higher concentration of 10 mg/mL, indicating that the Ti6Al4V surface has a strong adsorption interaction with the MSNs-NH2@PMPC. As a consequence, the adsorption of MSNs-NH2@PMPC forms a thin ad□sorption film on the Ti6Al4V

surface, which can function as a protective boundary film to achieve boundary lubrication between two sliding surfaces. In summary, the great reduction in both friction and wear of the tribological system, which is lubricated by MSNs-NH2@PMPC aqueous suspension, is contributed by combined effect of hydration lubrication and boundary lubrication.

Furthermore, the lubrication, rheology, and adsorption properties of the MSNs-NH2@PMPC aqueous suspension using phosphate buffer solution (PBS, pH = 7.4) at physiological condition were also performed in order to be meaningful in the context of applying to joints or to cells, and a similar result was obtained, as shown in Fig. S2.

It is calculated that the loading capacity (LC, %) and encapsulation efficiency (EE, %) of the DS-loaded MSNs-NH2@PMPC are ~3.9% and ~8.1%, which are greatly lower than that of DS-loaded MSNs (~8.8% and ~19.1%). It is noted that LC and EE are reduced after grafting the PMPC polymer brushes on the MSNs surface. The density of the PMPC polymer brushes should be decreased in order to further improve LC and EE, however, this will cause a reduction in lubrication property of the nanospheres. As a matter of fact, we have optimized the density of the PMPC polymer brushes for achieving both good lubrication and sustained drug release of the nanospheres. The drug release profiles of DS-loaded MSNs and DS-loaded MSNs-NH2@PMPC are shown in Fig. 4b. Both curves demonstrate an initial rapid drug release within 10 h, followed by a relative plateau stage afterward. At 72 h, 81.2% of DS is released from MSNs, which is much higher than that from MSNs□NH2@PMPC (40.6%). In addition, it is noted that the amount of DS released from MSNs-NH2@PMPC is remarkably lower than that from MSNs at all time intervals, which is attributed to the surface grafting of the PMPC polymer brushes onto the surface of MSNs, resulting in a sustained release behavior of the pre-loaded drug. DS that has been encapsulated into the mesopores of MSNs-NH2@PMPC can be gradually released due to the stretching of the hydrophilic PMPC polymer brushes in aqueous conditions, including for example the physiological environment of human joint. The drug loading and release properties of MSNs-NH2@PMPC indicate that the developed nanospheres, with PMPC polymer brushes acting as the “block”, can achieve sustained release of the pre-loaded drug when being locally and intra-articularly injected into the joint [46].

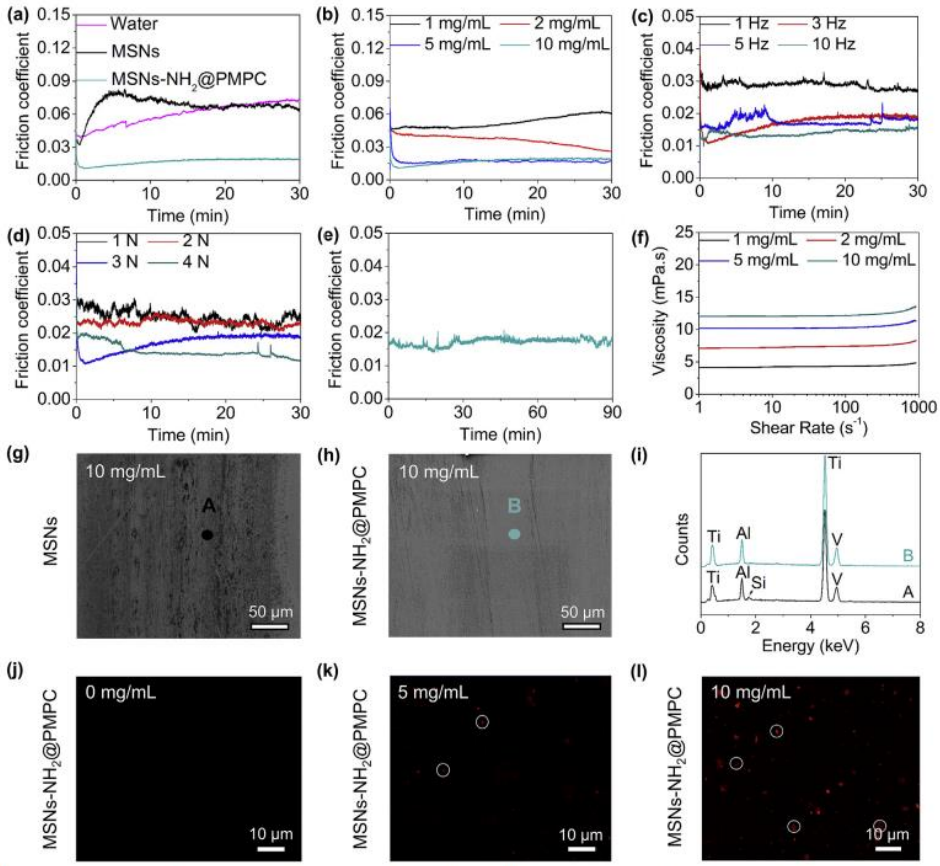

Fig. 3. Lubrication, rheology and adsorption properties of MSNs and MSNs-NH_2@PMPC aqueous suspensions. Lubrication properties of the nanospheres. Contact tribopairs: Ti6Al4V disk and polyethylene (PE) ball; reciprocating amplitude: 4 mm. (a) Friction coefficient-time plots of deionized water, MSNs and MSNs-NH_2@PMPC. (b–d) Friction coefficient-time plots of MSNs-NH_2@PMPC at three different test conditions including concentration, frequency and applied normal load. (e) Friction coefficient-time plot of MSNs-NH_2@PMPC with an extended test duration. (f) Rheological curves of MSNs-NH_2@PMPC at various concentrations showing a shear-thickening behavior. (g–i) SEM images and EDX analysis of the wear scar area (point A for MSNs and point B for MSNs-NH_2@PMPC) after the tribological test. (j–l) Fluorescence images of the Ti6Al4V surface incubated with RhB-labeled MSNs-NH_2@PMPC at different concentrations of 0 mg/mL, 5 mg/mL and 10 mg/mL.

3.4. In vitro cytotoxicity and mechanism for chondrocytes degradation protection

In vitro cytotoxicity and protection for chondrocytes degradation of the lubrication-enhanced and drug-delivered nanospheres (MSNsNH2@PMPC-DS) were investigated to evaluate the clinical application for the treatment of osteoarthritis, using MSNs and MSNs-NH2@PMPC as comparison groups. The results of Cell Counting Kit-8 (CCK-8) assay and Live/Dead staining assay of the MSNs, MSNs-NH2@PMPC and MSNs-NH2@PMPC-DS nanospheres incubated with the chondrocytes for 1, 3 and 5 days are demonstrated in Fig. 4c–e. The CCK-8 assay shows that the cell viability and proliferation of the chondrocytes are not highly affected by the nanospheres, and there is no significant difference between all the experimental groups and the control group at each time point (Fig. 4c). Additionally, the Live/Dead staining assay reveals that the chondrocytes are metabolically active, and few dead cells are observed at different time points (Fig. 4d). Furthermore, the number of viable cells increases with the culture time from day 1 to day 5, and still no significant difference is detected between all the experimental groups and the control group at different time points (Fig. 4e). The Live/Dead staining assay for an extended incubation of 14 days also demonstrates almost no dead cells (Fig. 4f). All the above results indicate that the nanospheres have excellent cell compatibility to the chondrocytes.

Chondrocytes are the sole cellular constituents of articular cartilage and are characteristic with dual-functions of regulating cartilage anabolism and catabolism via controlling synthesis of the two primary components of the matrix (i.e. collagen and proteoglycan) and enzymes that degrade

articular cartilage (e.g. matrix metalloproteinases). The pathogenesis of osteoarthritis involves many factors, but one well□documented change is chondrocytes degeneration, which results in an increased production of proteolytic enzymes. Although the exact mechanism by which the chondrocytes are activated has not been completely understood, several pathways may contribute to this process including mechanical stress, oxidative stress and inflammatory media□tors. In the present study, H2O2 is introduced to mimic the oxidative stress environment during the pathogenesis of osteoarthritis [47]. Basically, collagen II (Col2α) and aggrecan are two typical constituents of collagen and proteoglycan in the cartilage matrix. Following the treatment with H2O2, the mRNA expression levels of Col2α and aggrecan both decrease gradually with the intervention time (Fig. 5a and b). Subsequently, the protective effect of the nanospheres on chondrocytes degradation is examined. The quantitative real-time polymerase chain reaction (qRT-PCR) analyses indicate that the decrease in the mRNA expression levels of Col2α and aggrecan is reversed after addition of MSNs-DS and MSNs-NH2@PMPC-DS, both reaching over 50% of the control group (normal chondrocytes, Fig. 5c and d). However, the addition of MSNs and MSNs-NH2@PMPC has limited effect on increasing the mRNA expression levels of Col2α and aggrecan, which are quite similar to that of the blank group (the chondrocytes are solely treated with H2O2). Furthermore, the mRNA expression levels of MMP1 and tachykinin-1 (TAC1) are detected using qRT-PCR. MMP1 is one of the major cartilage-degrading enzymes resulting in breakdown of the cartilage matrix, and TAC1, as a neuropeptide expressed in many tis□sues, is related to pain signaling. The treatment with H2O2 causes a significant increase in the mRNA expression levels of MMP1 and TAC1 (the blank group versus the control group). Again, as expected, the addition of MSNs-DS and MSNs-NH2@PMPC-DS greatly reduces the mRNA expression levels of MMP1 and TAC1 in comparison with the blank group, while no obvious effect has been observed for MSNs and MSNs-NH2@PMPC (Fig. 5e and f).

The protein expression level of Col2α, as a representative, in chondrocytes treated with H2O2 and co-cultured with MSNs, MSNsNH2@PMPC and MSNs-NH2@PMPC-DS is examined by immunofluorescence staining. As demonstrated in Fig. 6, the protein expression level of Col2α is significantly reduced following treatment with H2O2 as the staining intensity of the blank group is visibly lower than that of the control group (Fig. 6a). The addition of MSNs and MSNs-NH2@PMPC also has limited effect on increasing the protein expression level of Col2α, while on the contrary a significant increase in the protein expression level of Col2α is observed by adding MSNs-NH2@PMPC-DS, in comparison with the blank group (Fig. 6b). The results of qRT-PCR and immunofluorescence staining reveal that the lubrication-enhanced and drug-delivered nanospheres MSNs-NH2@PMPC-DS developed in the present study can protect the oxidative stress-induced chondrocytes from degradation, which is achieved via a mechanism of up-regulating the anabolic components (Col2α, aggrecan) and down-regulating the catabolic proteases (MMP1) of articular cartilage. Additionally, MSNsNH2@PMPC-DS down-regulate the overexpression of pain-related gene (TAC1), which is desirably beneficial to alleviate the pain for the patients suffering from osteoarthritis. It should be noted that, as there is no friction or lubrication effect involved in the in vitro study, no obvious improvement is observed for the MSNs-NH2@PMPC group compared with the MSNs group and for the MSNs-NH2@PMPC-DS group compared with the MSNs-DS group.

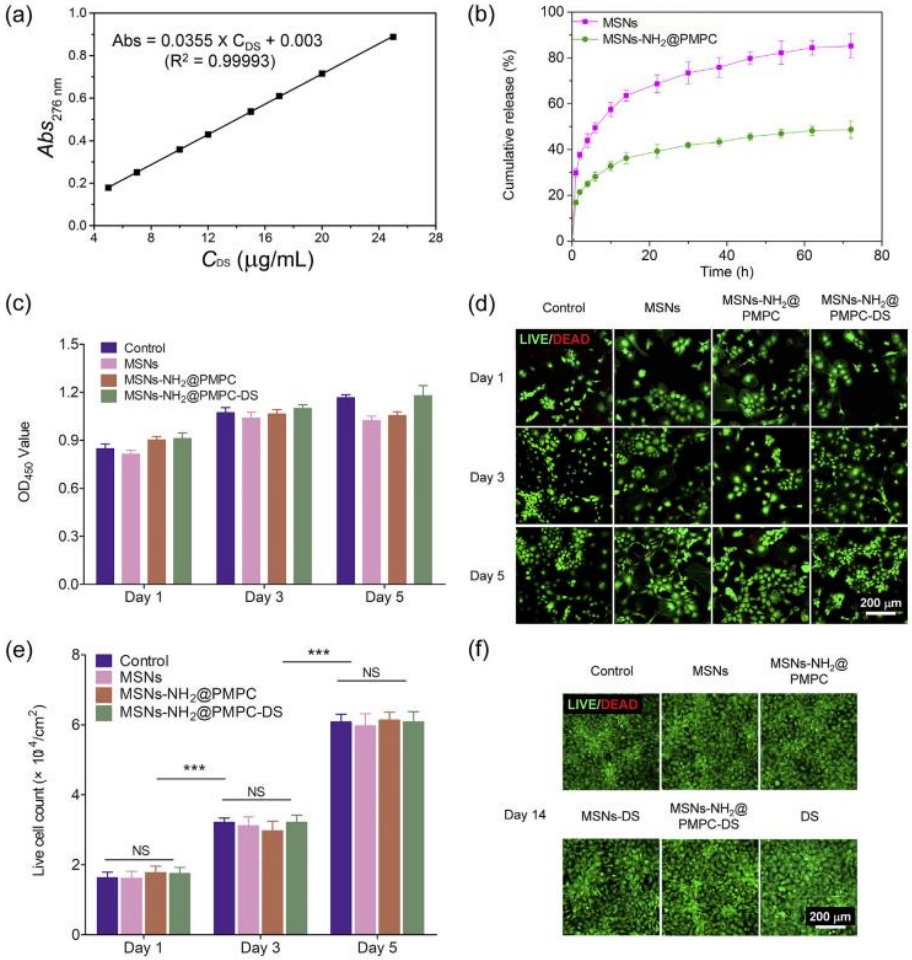

Fig. 4. Drug calibration curve, drug release and *in vitro* cytotoxicity of the nanospheres. (a) The calibration curve of DS with different concentrations. (b) The release profiles of the DS-loaded MSNs and DS-loaded MSNs-NH_2@PMPC in PBS (pH = 7.4) at 37 °C for 72 h. (c) *In vitro* cytotoxicity of MSNs, MSNs-NH_2@PMPC and MSNs-NH_2@PMPC-DS on chondrocytes detected by CCK-8 assay. (d) Representative fluorescence images displaying Live/Dead staining assay of chondrocytes co-cultured with MSNs, MSNs-NH_2@PMPC and MSNs-NH_2@PMPC-DS. (e) Viable cell count obtained from the Live/Dead staining assay. (f) Representative fluorescence images demonstrating Live/Dead staining assay of chondrocytes co-cultured with MSNs, MSNs-NH_2@PMPC, MSNs-DS, MSNs-NH_2@PMPC-DS, and DS for an extended incubation of 14 days. (n = 3, NS: no significance, ***P < 0.001).

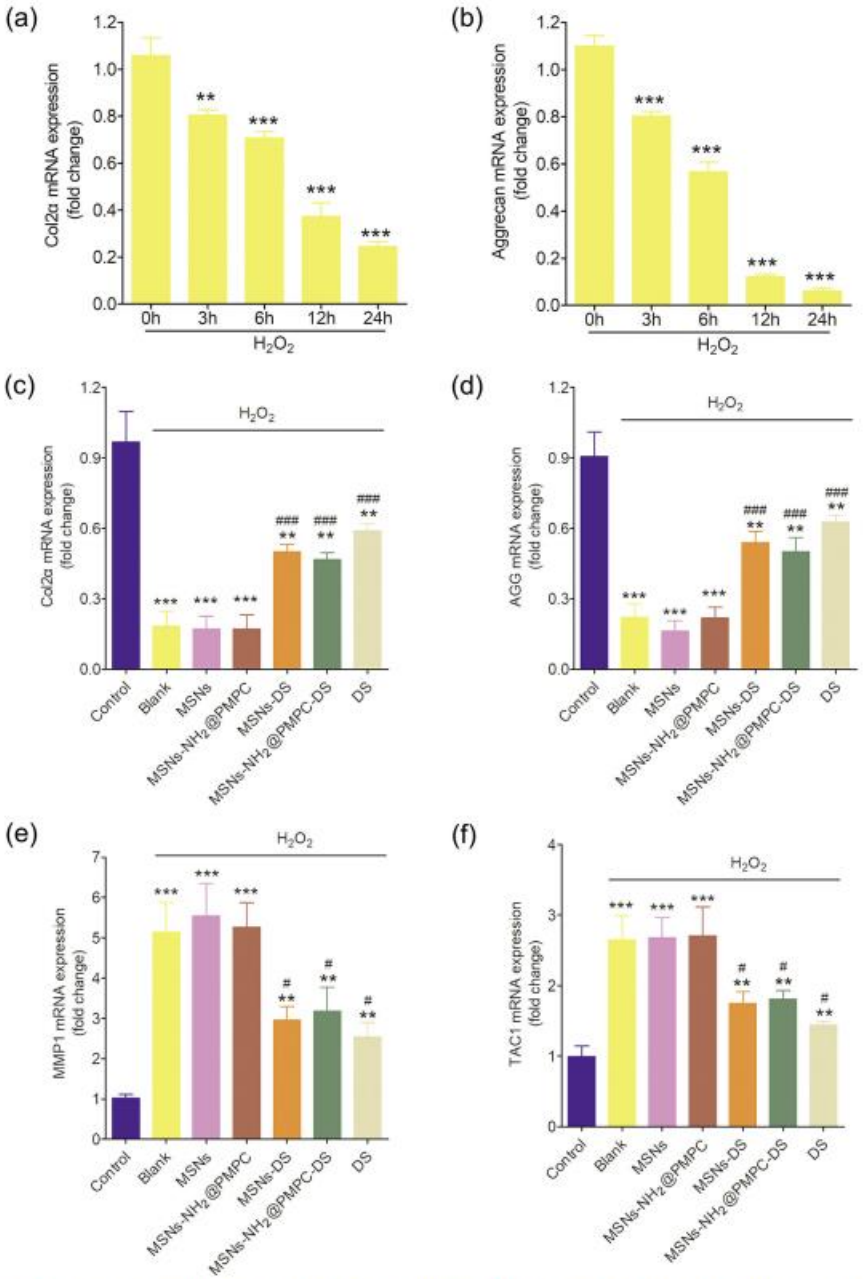

Fig. 5. Mechanism for chondrocytes degradation protection of the nanospheres. (a–b) The mRNA expression levels of (a) Col2α and (b) aggrecan in chondrocytes treated with H_2O_2 at various time points of 24 h. (c–f) The mRNA expression levels of (c) Col2α, (d) aggrecan, (e) MMP1 and (f) TAC1 in chondrocytes treated with H_2O_2 and co-cultured with MSNs, MSNs-NH_2@PMPC, MSN-DS, MSNs-NH_2@PMPC-DS and DS for 24 h (n = 3, the values are shown as mean ± standard deviation (SD), $^{**}P < 0.01$, $^{***}P < 0.001$, compared with the control group; $^{\#}P < 0.05$, $^{\#\#\#}P < 0.001$, compared with the blank group).

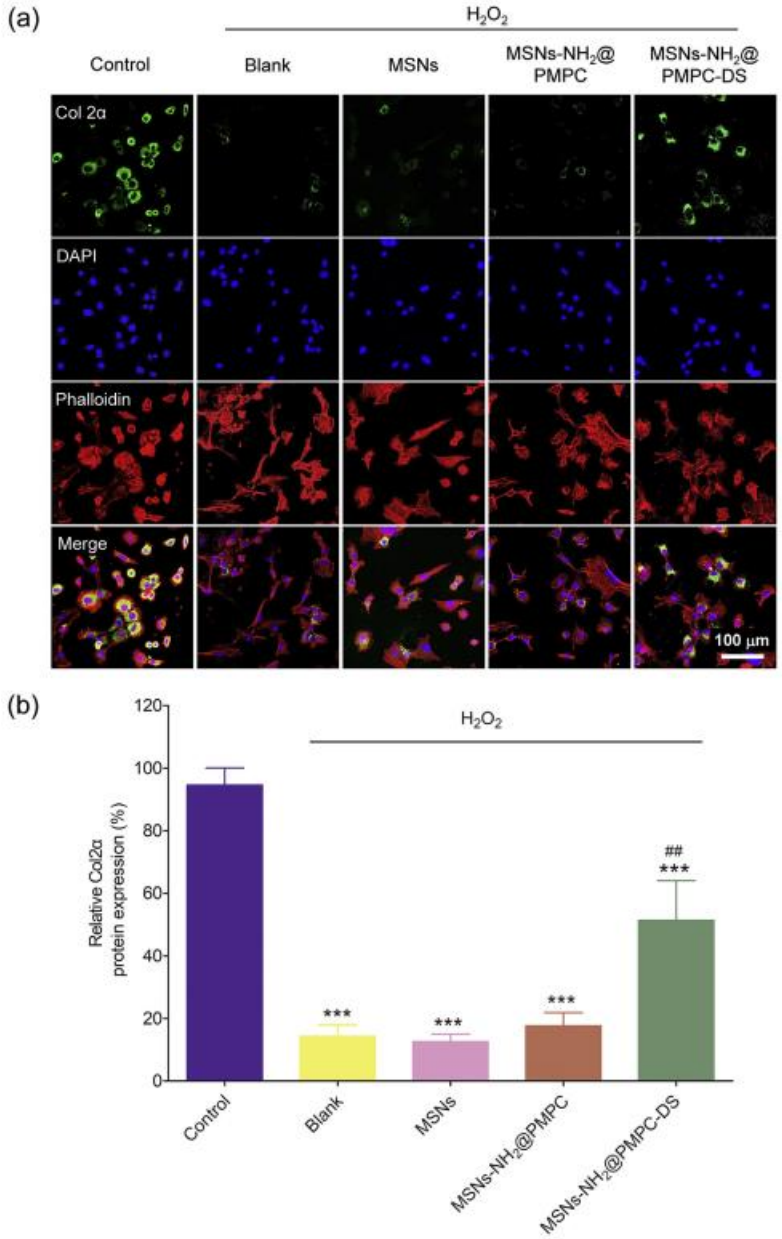

Fig. 6. Immunofluorescence staining. (a) Representative fluorescence images displaying the protein expression level of Col2α of chondrocytes treated with H_2O_2 and co-cultured with MSNs, MSNs-NH_2@PMPC and MSNs-NH_2@PMPC-DS for 12 h. Green: Molecular Probes labeling Col2α; Blue: DAPI labeling cell nuclei; Red: Phalloidin labeling cell actin. (b) The quantitative data showing the comparison of protein expression level of Col2α acquired based on the fluorescence intensity. (n = 3, $^{***}P < 0.001$, compared with the control group; $^{\#\#}P < 0.01$, compared with the blank group). (For interpretation of the references to colour in this figure legend, the reader is referred to the Web version of this article.)

3.5. In vivo synergetic treatment of osteoarthritis

A destabilization of the medial meniscus (DMM)-induced osteoarthritis model that has been commonly used in previous studies was established [48], and the in vivo synergetic treatment of osteoarthritis through intra-articularly injecting the lubrication-enhanced and drug□delivered nanospheres (MSNs-NH2@PMPC-DS) was evaluated by X-ray radiograph, micro-computed tomography (micro-CT) scanning and reconstruction, histological and immunohistochemistry staining.

The X-ray radiograph and articular space width of the rat knee joints are displayed in Fig. 7. At 2 weeks after the DMM surgery, the values of articular space width of the MSNs-DS, MSNs-NH2@PMPC and MSNsNH2@PMPC-DS groups are similar and significantly higher than that of the MSNs group. At 4 weeks after the DMM surgery, although the values of the four groups all decrease, the articular space width of the MSNsNH2@PMPC and MSNs-NH2@PMPC-DS groups is still significantly higher than that of the MSNs and MSNs-DS groups, respectively. Subsequently,

the rat knee joints are carefully detached and further examined based on micro-CT scanning and reconstruction, as shown in Fig. 8. At 2 weeks after the DMM surgery, the osteophyte volume of the MSNs-NH2@PMPC-DS group is significantly lower than that of the MSNs, MSNs-DS and MSNs-NH2@PMPC groups. At 4 weeks after the DMM surgery, the osteophyte volume of the four groups all increases, but the value of the MSNs-NH2@PMPC and MSNs-NH2@PMPC-DS groups is significantly lower than that of the MSNs and MSNs-DS groups, respectively. The above results clearly indicate that lubrication greatly contributes to inhibition of osteoarthritis development, and the best ourcome is obtained employing the nanospheres of MSNs-NH2@ PMPC-DS through synergetic treatment of enhanced lubrication and sustained drug delivery.

The representative histological evaluation of the cartilage tissues based on hematoxylin-eosin (H&E) staining and Safranin O-fast green staining is shown in Fig. 9a and b. For the MSNs group, typical features of osteoarthritis can be observed such as surface discontinuity, vertical fissure, erosion denudation and deformation. Compared with the MSNs group, the MSNs-DS, MSNs-NH2@PMPC and MSNs-NH2@PMPC-DS groups all demonstrate various degrees of improvement in morphological change, matrix staining and tidemark integrity promotion. The MSNs-NH2@PMPC-DS group best maintains the columnar architecture of cartilage, which is manifested as the preservation of higher cartilage thickness, less extensive erosion, decreased surface denudation and deformation, and increased tissue cellularity and cloning. Additionally, at 2 and 4 weeks after the DMM surgery, the MSNs-NH2@PMPC-DS group presents more intense Safranin O-fast green staining compared with the other groups (Fig. 9c), indicating that MSNs-NH2@PMPC-DS can effectively protect articular cartilage during the development of osteoarthritis in terms of glycosaminoglycan (GAG) deposition, retention of cartilage thickness, and attenuation of cartilage matrix depletion. Furthermore, the result of Osteoarthritis Research Society International (OARSI) score as displayed in Fig. 9d shows that there is a significant reduction in the value for the MSNs-NH2@PMPC-DS group compared with the other groups at 2 and 4 weeks after the DMM surgery. The protein expression level of Col2α in chondrocytes of the cartilage tissues is detected via immunohistochemistry staining, and the result is shown in Fig. 10. At 2 and 4 weeks after the DMM surgery, the relative protein expression level of Col2α of the MSNs-NH2@PMPC and MSNs-NH2@PMPC-DS groups is significantly higher than that of the MSNs and MSNs-DS groups, respectively. Specifically, at both time points the MSNs-NH2@PMPC-DS group has the highest relative protein expression level of Col2α. The above results clearly indicate that the lubrication-enhanced and drug-delivered nanospheres of MSNs-NH2@ PMPC-DS can effectively inhibit the development of osteoarthritis.

In order to investigate the effect of the lubrication-enhanced and drug-delivered nanospheres (MSNs-NH2@PMPC-DS) on the treatment of osteoarthritis at different stages, a repeated in vivo experiment was performed by intra-articularly injecting PBS, MSNs, MSNs-NH2@PMPC and MSNs-NH2@PMPC-DS, and the results of the X-ray radiograph, micro-CT arthrography, histological staining and immunohistochemistry staining were collected at 8 weeks after the DMM surgery, as shown in Figs. S3–S5. The X-ray radiograph indicates that the articular space width of the PBS group is slightly lower than that of the other three groups (including MSNs, MSNs-NH2@PMPC and MSNs□NH2@PMPC-DS), although the difference is not significant. The micro□CT arthrography demonstrates that the osteophyte volumes of the PBS, MSNs and MSNs-NH2@PMPC groups are similar, and a significantly decreased value is observed for the MSNs-NH2@PMPC-DS group. The histological staining and immunohistochemistry staining also show

that the relative GAG content, OARSI score and protein expression level of Col2α for the PBS, MSNs and MSNs-NH2@PMPC groups are similar, and a significant difference is obtained for the MSNs-NH2@PMPC-DS group. Overall, the results indicate that the efficacy of lubrication, which is achieved by grafting the PMPC polymer brushes onto the surface of MSNs, is compromised on the inhibition of late stage osteoarthritis (In the present study, the development of osteoarthritis for the rats is accelerated via running train). It is considered that this phenomenon is attributed to the nature of osteoarthritis. As a progressive and irreversible joint disease, the pathological process of osteoarthritis becomes increasingly severe over time, and thus the enhanced lubrication contributes to the inhibition of osteoarthritis at an early stage, whereas for late stage osteoarthritis it can only be effectively treated through drug intervention, herein using the nanosphere MSNs-NH2@PMPC-DS.

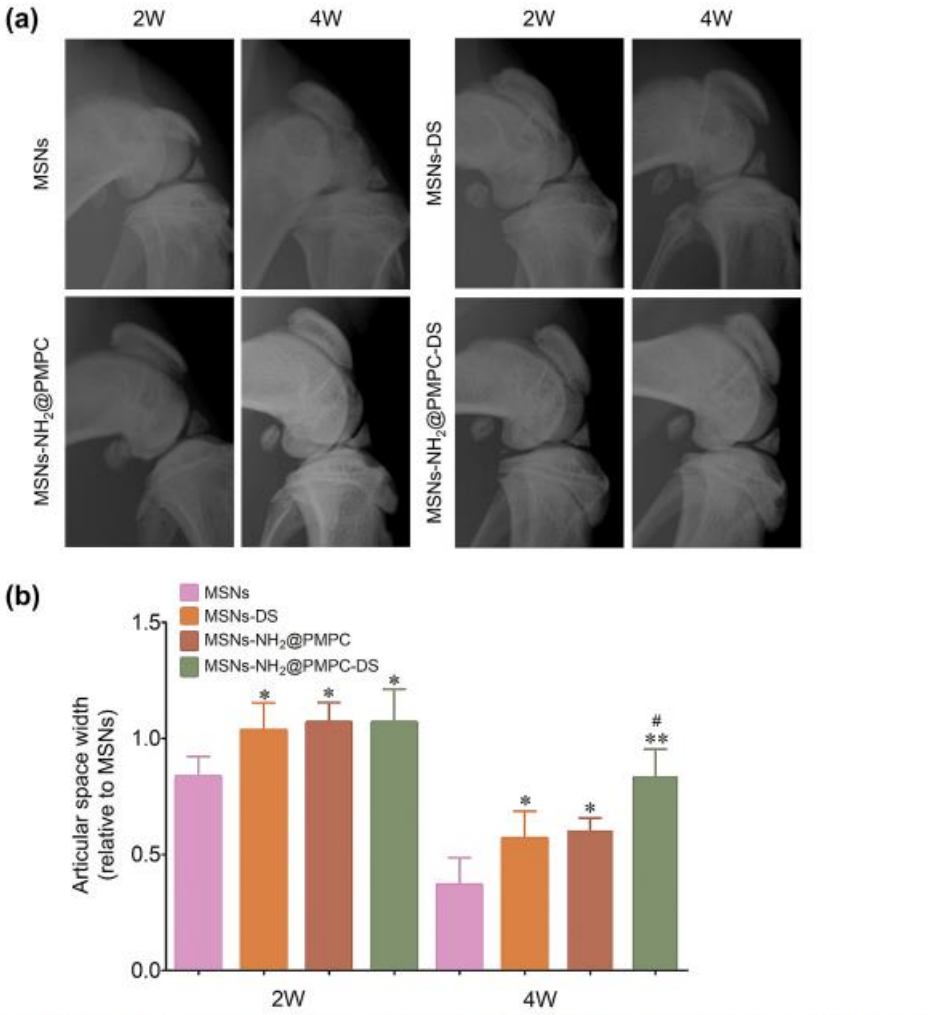

Fig. 7. X-ray radiography. (a) At 2 and 4 weeks after the DMM surgery, representative X-ray radiographs of rat knee joints receiving the intra-articular injections of MSNs, MSNs-DS, MSNs-NH_2@PMPC and MSNs-NH_2@PMPC-DS for the treatment of DMM-induced osteoarthritis. (b) Articular space width of rat knee joints measured from the X-ray radiographs. ($n = 3$, $^{*}P < 0.05$, $^{**}P < 0.01$, compared with the MSNs group; $^{\#}P < 0.05$, compared with the MSNs-DS group).

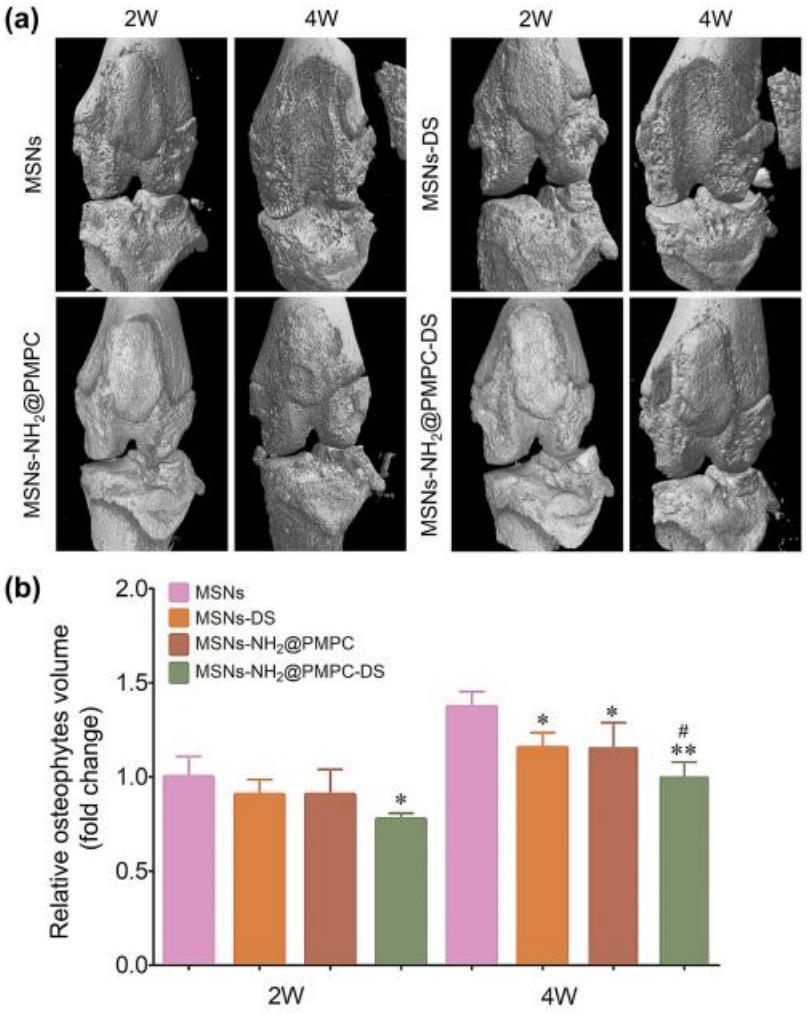

Fig. 8. Micro-CT arthrography. (a) At 2 and 4 weeks after the DMM surgery, representative micro-CT scanning and reconstruction of rat knee joints receiving the intra-articular injection of MSNs, MSNs-DS, MSNs-NH_2@PMPC and MSNs-NH_2@PMPC-DS for the treatment of DMM-induced osteoarthritis. (b) The relative osteophytes volume of the experimental groups. (n = 3, the values are shown as mean ± SD, $^{*}P < 0.05$, $^{**}P < 0.01$, compared with the MSNs group; $^{\#}P < 0.05$, compared with the MSNs-DS group).

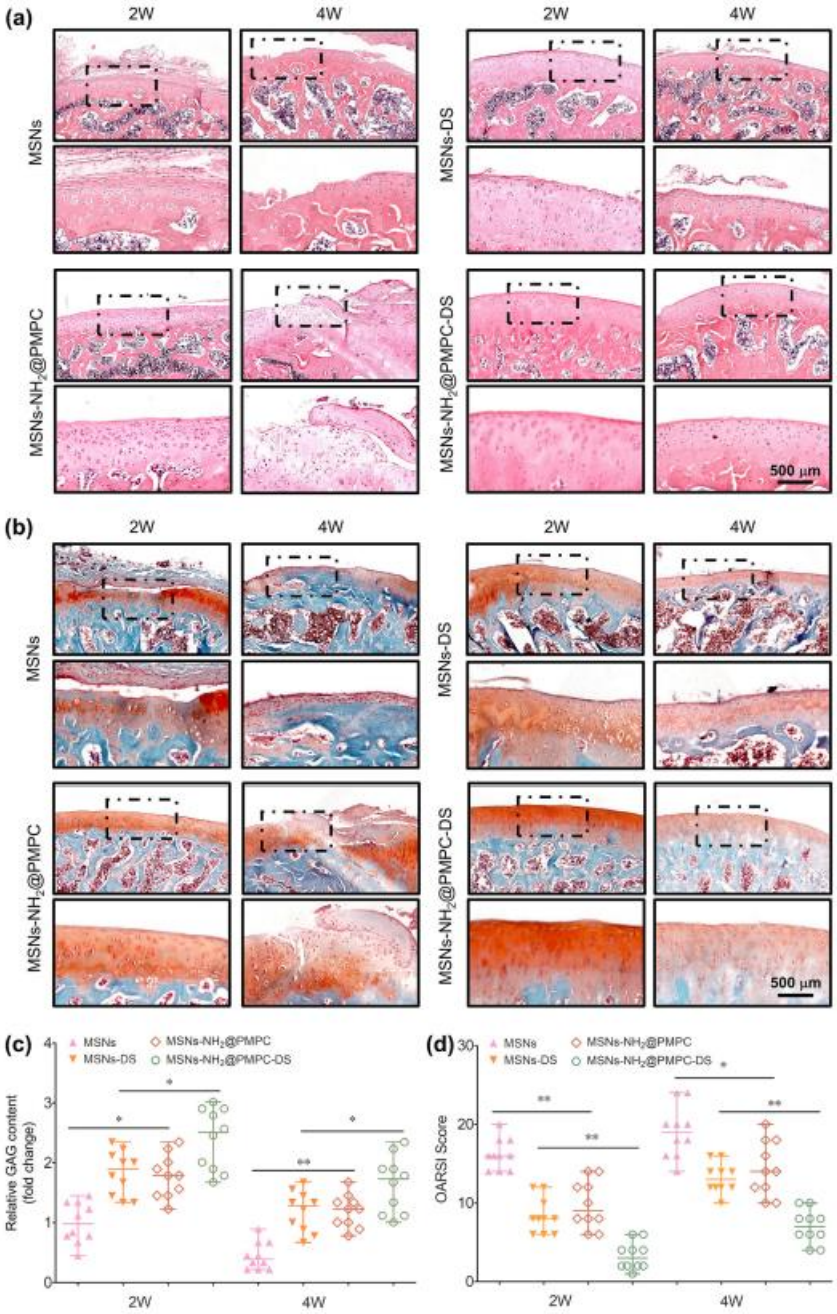

Fig. 9. Histological staining. (a–b) Representative (a) H&E staining and (b) Safranin O-fast green staining of the cartilage sections for the MSNs, MSNs-DS, MSNs-NH_2@PMPC and MSNs-NH_2@PMPC-DS groups following treatment of rat DMM-induced osteoarthritis at 2 and 4 weeks after surgery. (c) Quantification of relative GAG content to the MSNs group at 2 and 4 weeks after surgery, obtained from the Safranin O-fast green staining of the cartilage sections. (d) OARSI score of articular cartilage for each group following treatment of rat DMM-induced osteoarthritis at 2 and 4 weeks after surgery. (n = 10, $^{*}P < 0.05$, $^{**}P < 0.01$). (For interpretation of the references to colour in this figure legend, the reader is referred to the Web version of this article.)

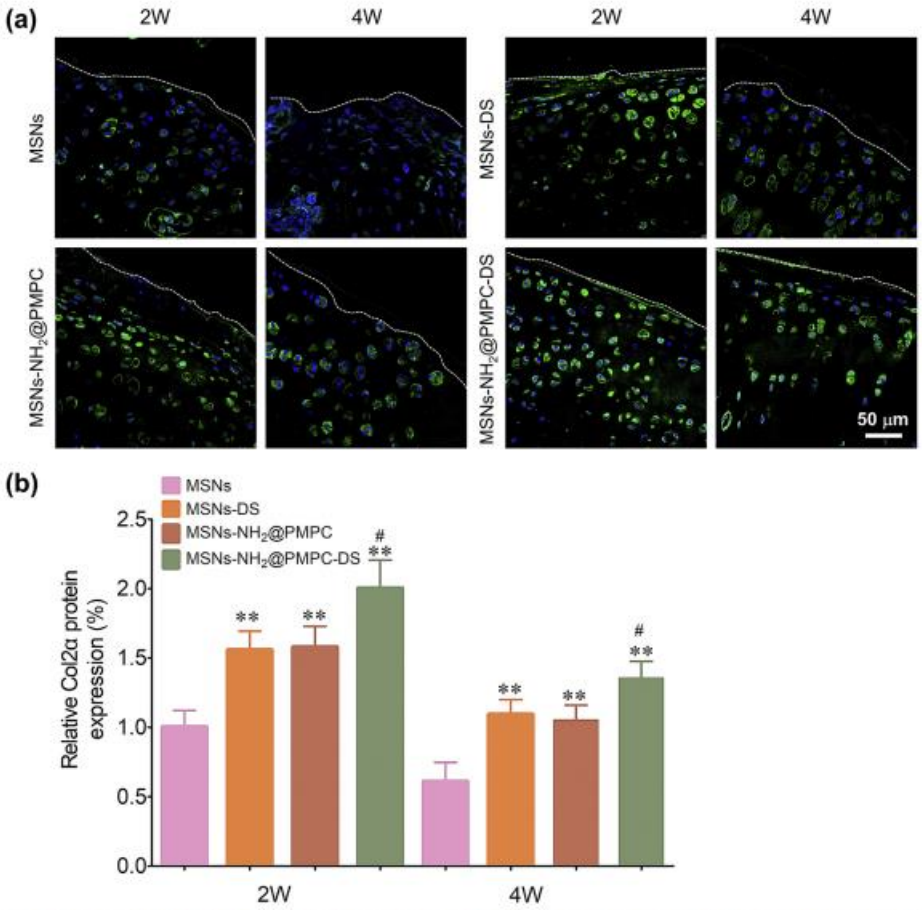

Fig. 10. Immunohistochemistry staining. (a) Representative fluorescence images displaying the protein expression level of Col2α in the articular cartilage of rat knees treated by MSNs, MSNs-DS, MSNs-NH_2@PMPC and MSNs-NH_2@PMPC-DS at 2 and 4 weeks after the DMM surgery. Green: Molecular Probes labeling Col2α; Blue: DAPI labeling cell nuclei. (b) The quantitative data showing the comparison of protein expression level of Col2α acquired based on the fluorescence intensity. (n = 5, the values are presented as mean ± SD, $^{**}P < 0.01$, compared with the MSNs group; $^{\#}P < 0.05$, compared with the MSNs-DS group). (For interpretation of the references to colour in this figure legend, the reader is referred to the Web version of this article.)

4. Conclusions

In this study, inspired by the superlubrication property of articular cartilage, specifically the hydration lubrication mechanism of the zwitterionic charges in phosphatidylcholine lipid, we successfully designed and developed biomimetic superlubricated drug-loaded nano□spheres (MSNs-NH2@PMPC-DS) by photopolymerization of PMPC polymer brushes onto the surface of the drug nanocarriers MSNs. The PMPC polymer brushes with the same zwitterionic charges as phosphatidylcholine lipid significantly enhanced lubrication, and thnanocarriers MSNs achieved sustained drug delivery by encapsulating an anti-inflammatory drug DS, therefore the nanospheres developed herein could represent a promising strategy for synergetic treatment of osteoarthritis. The tribological and drug loading-release experiments revealed greatly improved lubrication property and sustained drug re□lease behavior of the nanospheres. Additionally, the in vitro and in vivo experiments showed that the biocompatible nanospheres not only protected oxidative stress-induced chondrocytes from degradation but also inhibited the development of osteoarthritis based on an animal DMM model. The mechanism was attributed to up-regulation of anabolic components and down-regulation of catabolic proteases of the articular cartilage. Importantly, the expression of pain-related gene was decreased upon the use of the nanospheres. In summary, the super□lubricated drug-loaded nanospheres, MSNs-NH2@PMPC-DS, could be potentially used as an intra-articularly injected nanomedicine for the treatment of osteoarthritis.

CRediT authorship contribution statement

Hao Chen: Methodology, Investigation, Writing - original draft. Tao Sun: Methodology, Investigation, Writing - original draft. Yufei Yan: Methodology, Investigation, Writing - original draft. Xiuling Ji: Formal analysis. Yulong Sun: Methodology, Formal analysis. Xin Zhao: Visualization. Jin Qi: Formal analysis. Wenguo Cui: Conceptualization, Funding acquisition, Writing - review & editing. Lianfu Deng: Resources, Funding acquisition. Hongyu Zhang: Conceptualization, Resources, Writing - review & editing, Funding ac□quisition.

Declaration of competing interest

The authors declare that they have no competing interests.

Acknowledgements

This study was financially supported by National Natural Science Foundation of China (51675296, 81972134, 81702125), Tsinghua University Initiative Scientific Research Program (20197050026), Tsinghua University-Peking Union Medical College Hospital Initiative Scientific Research Program (20191080593), Shanghai Municipal Education Commission—Gaofeng Clinical Medicine Grant Support (20171906), Shanghai Jiao Tong University "Medical and Research" Program (ZH2018ZDA04), Science and Technology Commission of Shanghai Municipality (18ZR1434200, 19440760400), and Ng Teng Fong Charitable Foundation (202-276-132-13).

References

[1] S. Jahn, J. Klein, Lubrication of articular cartilage, Phys. Today 71 (2018) 48–52.

[2] J. Seror, L. Zhu, R. Goldberg, A.J. Day, J. Klein, Supramolecular synergy in the boundary lubrication of synovial joints, Nat. Commun. 6 (2015) 6497.

[3] L.R. Ma, A. Gaisinskaya-Kipnis, N. Kampf, J. Klein, Origins of hydration lubrication, Nat. Commun. 6 (2015) 6060.

[4] J. Klein, Repair or replacement: a joint perspective, Science 323 (2009) 47–48.

[5] S. Jahn, J. Seror, J. Klein, Lubrication of articular cartilage, Annu. Rev. Biomed. Eng. 18 (2016) 235–258.

[6] T.L. Vincent, Targeting mechanotransduction pathways in osteoarthritis: a focus on the pericellular matrix, Curr. Opin. Pharmacol. 13 (2013) 449–454.

[7] A. Burleigh, A. Chanalaris, O. Boruc, J. Saklatvala, T.L. Vincent, Fgf2 is a me□chanotransducer in destabilised joints in vivo, Int. J. Exp. Pathol. 93 (2012) 23–24.

[8] G. Morgese, E. Cavalli, M. Muller, M. Zenobi-Wong, E.M. Benetti, Nanoassemblies of tissue-reactive, polyoxazoline graft-copolymers restore the lubrication properties of degraded cartilage, ACS Nano 11 (2017) 2794–2804.

[9] S. Lue, S. Koppikar, K. Shaikh, D. Mahendira, T.E. Towheed, Systematic review of non-surgical therapies for osteoarthritis of the hand: an update, Osteoarthritis Cartilage 25 (2017) 1379–1389.

[10] W.E. Krause, E.G. Bello, R.H. Colby, Rheology of sodium hyaluronate under phy□siological conditions, Biomacromolecules 2 (2001) 65–69.

[11] J. Salazar, L. Bello, M. Chávez, R. Añez, J. Rojas, V. Bermúdez, Glucosamine for osteoarthritis: biological effects, clinical efficiency, and safety on glucose metabo lism, Arthritis (2014) 1–13 2014.

[12] G. Liu, M. Cai, F. Zhou, W. Liu, Charged polymer brushes-grafted hollow silica nanoparticles

as a novel promising material for simultaneous joint lubrication and treatment, J. Phys. Chem. 118 (2014) 4920–4931.
[13] T. Sun, Y.L. Sun, H.Y. Zhang, Phospholipid-coated mesoporous silica nanoparticles acting as lubricating drug nanocarriers, Polymers 10 (2018) 513.
[14] J. Klein, Hydration lubrication, Friction 1 (2013) 1–23.
[15] T. Moro, Y. Takatori, K. Ishihara, T. Konno, Y. Takigawa, T. Matsushita, U. Chung, K. Nakamura, H. Kawaguchi, Surface grafting of artificial joints with a biocompa□tible polymer for preventing periprosthetic osteolysis, Nat. Mater. 3 (2004) 829–836.
[16] M. Kyomoto, T. Moro, Y. Takatori, H. Kawaguchi, K. Nakamura, K. Ishihara, Self□initiated surface grafting with poly(2-methacryloyloxyethyl phosphorylcholine) on poly(ether-ether-ketone), Biomaterials 31 (2010) 1017–1024.
[17] M. Kyomoto, T. Moro, K. Saiga, F. Miyaji, H. Kawaguchi, Y. Takatori, K. Nakamura, K. Ishihara, Lubricity and stability of poly(2-methacryloyloxyethyl phosphor□ylcholine) polymer layer on CoCrMo surface for hemi-arthroplasty to prevent de□generation of articular cartilage, Biomaterials 31 (2010) 658–668.
[18] U. Raviv, S. Giasson, N. Kampf, J.F. Gohy, R. Jerome, J. Klein, Lubrication by charged polymers, Nature 425 (2003) 163–165.
[19] M. Chen, W. Briscoe, S.P. Armes, J. Klein, Lubrication at physiological pressures by polyzwitterionic brushes, Science 323 (2009) 1698–1701.
[20] J.L. Paris, M.V. Cabañas, M. Manzano, M. Vallet-Regi, Polymer-grafted mesoporous silica nanoparticles as ultrasound-responsive drug carriers, ACS Nano 9 (2015) 11023–11033.
[21] X. Wu, Z. Wang, D. Zhu, S. Zong, L. Yang, Y. Zhong, Y. Cui, pH and thermo dual□stimuli-responsive drug carrier based on mesoporous silica nanoparticles en□capsulated in a copolymer-lipid bilayer, ACS Appl. Mater. Interfaces 5 (2013) 10895–10903.
[22] J. Zhang, Z. Yuan, Y. Wang, W. Chen, G. Luo, S. Cheng, R. Zhuo, X. Zhang, Multifunctional envelope-type mesoporous silica nanoparticles for tumor-triggered targeting drug delivery, J. Am. Chem. Soc. 135 (2013) 5068–5073.
[23] Q. Li, Y.F. Sun, Y.L. Sun, J. Wen, Y. Zhou, Q. Bing, L.D. Isaacs, Y. Jin, H. Gao, Y. Yang, Mesoporous silica nanoparticles coated by layer-by-layer self-assembly using cucurbit (7) Uril for in vitro and in vivo anticancer drug release, Chem. Mater. 26 (2014) 6418–6431.
[24] H. Oveisi, S. Rahighi, X.F. Jiang, Y. Nemoto, A. Beitollahi, S. Wakatsuki, Y. Yamauchi, Unusual antibacterial property of mesoporous titania films: drastic improvement by controlling surface area and crystallinity, Chem. Asian J. 5 (2010) 1978–1983.
[25] B.P. Bastakoti, S. Ishihara, S.Y. Leo, K. Ariga, K.C.W. Wu, Y. Yamauchi, Polymeric micelle assembly for preparation of large-sized mesoporous metal oxides with various compositions, Langmuir 30 (2014) 651–659.
[26] Y. Yamauchi, T. Nagaura, A. Ishikawa, T. Chikyow, S. Inoue, Evolution of standing mesochannels on porous anodic alumina substrates with designed conical holes, J. Am. Chem. Soc. 130 (2008) 10165–10170.
[27] C.W. Wu, Y. Yamauchi, T. Ohsuna, K. Kuroda, Structural study of highly ordered mesoporous silica thin films and replicated Pt nanowires by high-resolution scan□ning electron microscopy (HRSEM), J. Mater. Chem. 16 (2006) 3091–3098.
[28] M. Nandi, J. Mondal, K. Sarkar, Y. Yamauchi, A. Bhaumik, Highly ordered acid functionalized SBA-15: a novel organocatalyst for the preparation of xanthenes, Chem. Commun. 47 (2011) 6677–

6679.
[29] J. Liu, B. Wang, S.B. Hartono, T.T. Liu, P. Kantharidis, A.P.J. Middelberg, G.Q. Lu, L.Z. He, S.Z. Qiao, Magnetic silica spheres with large nanopores for nucleic acid adsorption and cellular uptake, Biomaterials 33 (2012) 970–978.
[30] J.S. Gao, S.C. Wu, F. Tan, H. Tian, J. Liu, G.Q. Lu, Nanoengineering of amino□functionalized mesoporous silica nanospheres as nanoreactors, Prog. Nat. Sci-Mater 28 (2018) 242–245.
[31] J. Liu, T.T. Liu, J. Pan, S.M. Liu, G.Q. Lu, Advances in multicompartment meso□porous silica micro/nanoparticles for theranostic applications, Annu. Rev. Chem. Biomol. Eng. 9 (2018) 389–411.
[32] Z. Li, J.C. Barnes, A. Bosoy, J.F. Stoddart, J.I. Zink, Mesoporous silica nanoparticles in biomedical applications, Chem. Soc. Rev. 41 (2012) 2590–2605.
[33] Y.F. Yan, T. Sun, H.B. Zhang, X.L. Ji, Y.L. Sun, X. Zhao, L.F. Deng, Q. Jin, W.G. Cui, H.A. Santos, H.Y. Zhang, Euryale ferox seed-inspired super-lubricated nanoparticles for treatment of osteoarthritis, Adv. Funct. Mater. 29 (2019) 1807559.
[34] M. Kyomoto, T. Moro, S. Yamane, M. Hashimoto, Y. Takatori, K. Ishihara, Poly (ether-ether-ketone) orthopedic bearing surface modified by self-initiated surface grafting of poly(2-methacryloyloxyethyl phosphorylcholine), Biomaterials 34 (2013) 7829–7839.
[35] D. Shi, X. Xu, Y. Ye, K. Song, Y. Cheng, J. Di, Q. Hu, J. Li, H. Ju, Q. Jiang, Z. Gu, Photo-cross-linked scaffold with kartogenin-encapsulated nanoparticles for carti□lage regeneration, ACS Nano 10 (2016) 1292–1299.
[36] Y. Sun, Q. Li, Y. Zhou, Y. Yang, Enzyme-responsive supramolecular nanovalves crafted by mesoporous silica nanoparticles and choline-sulfonatocalix[4]arene [2] pseudorotaxanes for controlled cargo release, Chem. Commun. 49 (2013) 9033–9035.
[37] Y. Sun, Y. Yang, D. Chen, G. Wang, Y. Zhou, C. Wang, J.F. Stoddart, Mechanized silica nanoparticles based on pillar[5]arenes for on-command cargo release, Small 9 (2013) 3224–3229.
[38] F. Sun, Y. Li, N. Zhang, J. Nie, Initiating gradient photopolymerization and migration of a novel polymerizable polysiloxane α-hydroxy alkylphenones photoinitiator, Polymer 55 (2014) 3656–3665.
[39] H. Zhang, Y. Zhu, X. Hu, Y. Sun, Y. Sun, J. Han, Y. Yan, M. Zhou, An investigation on the biotribocorrosion behaviour of CoCrMo alloy grafted with polyelectrolyte brush, Bio Med. Mater. Eng. 24 (2014) 2151–2159.
[40] Y. Jiao, S. Liu, Y. Sun, W. Yue, H. Zhang, Bioinspired surface functionalization of nanodiamonds for enhanced lubrication, Langmuir 34 (2018) 12436–12444.
[41] K.P.H. Pritzker, S. Gay, S.A. Jimenez, K. Ostergaard, J.P. Pelletier, P.A. Revell, D. Salter, W.B. van den Berg, Osteoarthritis cartilage histopathology: grading and staging, Osteoarthritis Cartilage 14 (2006) 13–29.
[42] Y. Zhang, C. Ang, M. Li, S. Tan, Q. Qu, Z. Luo, Y. Zhao, Polymer-coated hollow mesoporous silica nanoparticles for triple-responsive drug delivery, ACS Appl. Mater. Interfaces 7 (2015) 18179–18187.
[43] C. Boyer, N.A. Corrigan, K. Jung, D. Nguyen, T. Nguyen, N.M. Adnan, S. Oliver, S. Shanmugam, J. Yeow, Copper-mediated living dadical polymerization (atom transfer radical polymerization and copper (0) mediated polymerization): from fundamentals to Bioapplications, Chem. Rev. 116 (2016) 1803–1949.
[44] H. Zhang, S. Zhang, J. Luo, Y. Liu, S. Qian, Investigation of protein adsorption mechanism and biotribological properties at simulated stem-cement interface, J. Tribol. 135 (2013) 032301.
[45] H. Zhang, J. Luo, M. Zhou, Y. Zhang, Y. Huang, Biotribological properties at the stem-cement

interface lubricated with different media, J. Mech. Behav. Biomed. Mater. 20 (2013) 209–216.
[46] Y. Sun, Y. Sun, L. Wang, J. Ma, Y. Yang, H. Gao, Nanoassembles constructed from mesoporous silica nanoparticles and surface-coated multilayer polyelectrolytes for controlled drug delivery, J. Micro. Meso. 185 (2014) 245–253.
[47] M.R. Ahmed, A. Mehmood, F.-ur-R. Bhatti, S.N. Khan, S. Riazuddin, Combination of ADMSCs and chondrocytes reduces hypertrophy improves the functional properties of osteoarthritic cartilage, Osteoarthritis Cartilage 22 (2014) 1894–1901.
[48] H. Iijima, T. Aoyama, A. Ito, J. Tajino, M. Nagai, S. Zhang, S. Yamaguchi, H. Kuroki, Destabilization of the medial meniscus leads to subchondral bone defects and sitespecific cartilage degeneration in an experimental rat model, Osteoarthritis Cartilage 22 (2014) 1036–1043